Available online at www.sciencedirect.com

ScienceDirect

Advances in Space Research 69 (2022) 3514–3524

ADVANCES IN SPACE RESEARCH (a COSPAR publication)

www.elsevier.com/locate/asr

Cosmic ray observations from Livingston Island ☆

Juan José Blanco [a,*], Juan Ignacio García-Tejedor [a], Óscar García-Población [a], Sindulfo Ayuso [a], Alejandro López-Comazzi [a], Iván Vrublevskyy [a], Manuel Prieto [a], Anna Morozova [b]

[a] University of Alcalá, Plaza San Diego s/n, Alcalá de Henares 28801, Spain
[b] Instituto de Astrofísica e Ciências do Espaço, Universidade Coimbra, Portugal

Received 18 August 2021; received in revised form 21 February 2022; accepted 23 February 2022
Available online 4 March 2022

Abstract

ORCA, from the Spanish name *Observatorio de Rayos Cósmicos Antártico*, is a cosmic ray detector devoted to the observation of secondary cosmic rays at Juan Carlos I Spanish Antarctic Base ($62^\circ\ 39'\ 46''\ S, 60^\circ\ 23'\ 20''\ W$, 12 m above sea level). ORCA was installed at the beginning of January 2019 after performing a latitudinal survey from Vigo (Spain) to Livingston Island aboard the Sarmiento de Gamboa Research Vessel. ORCA was in commissioning phase from January 2019 to March 2020, being in normal operation mode from March 2020. A vertical cutoff rigidity of $2.37\,GV$ has been computed at ORCA location and during the first year of operation, i. e. from March 2020 to March 2021.

ORCA consists of three detectors stacked in a shared structure that maintains the relative distances between the detectors. A muon telescope (ORCM), a neutron monitor without any shielding around (ORCB) and a 3NM64 neutron monitor (ORCA). This configuration allows the measurement of neutron count rates at two different energy thresholds, muon count rate and muon incident directions.

Measurements recorded during the first year of operation and ORCA potential capabilities are shown in this work.

Keywords: Cosmic rays; Neutron monitors; Muon telescopes; Sun-Earth relationship

1. Introduction

The Earth is immersed in a continuous flux of cosmic rays with energies ranging from 10^7 eV/nucleon to 10^{20} eV/nucleon. Moreover, the cosmic ray flux varies from 1 particle per m^2 and second to 1 particle per square kilometer and century. The primary cosmic ray differential spectrum follows a power law in energy with a spectral index of about -2.7. Below ~ 1 GeV/nucleon, the differential spectrum is no longer a simple power law reaching a maximum at some hundreds of MeV/nucleon. Cosmic ray flux at Earth's orbit is affected by the solar activity below some tens of GeV/nucleon. For this reason, temporal variations in the cosmic ray flux can be used as indicator of solar activity. These variations are observed by instruments at ground level such as neutron monitors which observe secondary cosmic rays (mainly neutrons) produced by cosmic rays at the top of the atmosphere (Smart and Shea, 1988).

The magnetosphere acts as a filter for particle magnetic rigidities, ranging from 0 GV on the magnetic poles up to 20 GV above the Indonesian peninsula. Moreover, the atmosphere also acts as an energy filter, being cosmic ray energy loss strongly dependent on the traversed atmospheric thickness. These effects can be used to measure the cosmic ray spectrum at this energy range by installing cosmic ray detectors, such as neutron monitors or muon

☆ ORCA.

* Corresponding author.
E-mail address: juanjo.blanco@uah.es (J.J. Blanco).

https://doi.org/10.1016/j.asr.2022.02.046
0273-1177/

telescopes, at different geomagnetic locations and altitudes above sea level.

Using Earth as a giant cosmic ray detector drives international collaborations to build global networks of these detectors. The neutron monitor data base (NMDB) is an example of this. NMDB provides access to real-time and historical data to neutron monitor measurements from stations around the world (https://www.nmdb.eu/). Every station integrated into the network can be identified by four capital letters. For instance, the Castilla La Mancha Neutron monitor (CaLMa) is referred as CALM in the NMDB (Medina et al., 2013). Global coverage is one of the aims of NMDB, and new stations should fill the gaps in the current network. The Antarctic Peninsula is one of this gaps since LARC neutron monitor, which was operative at King George Island, in the South Shetland Archipielago, was switched off (Cordaro et al., 2012).

The Juan Carlos I Spanish Antarctic Base (BAE-JCI) is in Livingston Island, $62°39'46''S, 60°23'20''W$ at 12 m above sea level (a.s.l.), which is also in the South Shetland Archipielago 134 km away from King George Island. The station is built in a beach on the initial slopes of Mount Sofía (275 m altitude) next to Española cove. Livingston Island is strongly glaciated, and Mount Sofia is at the border of Johnson's glacier. The BAE-JCI is a summer research station, i.e. it is only open during the antarctic summer, from mid-November to the beginning of March, typically. Currently, the BAE-JCI facilities supply standard power and communications infrastructure for running experiments during the summer, but both power and communications are very limited in winter, once the BAE-JCI is closed.

The BAE-JCI was at averaged effective vertical cutoff rigidity of $R = 2.37\,GV$ from March 2020 to March 2021. This value results from the Izmiran calculator at https://tools.izmiran.ru/cutoff2050/ (Belov et al., 2021). In this calculation the following conditions have been set. A cosmic ray flat spectrum, the International Geomagnetic Reference Field (IGRF-12) for the magnetosphere (Thébault et al., 2015) and the Tsyganenko model to account the induced external magnetic field (Tsyganenko, 1989). A Kp-index of 0 has been used to take into account a magnetosphere in calm. Vertical cosmic ray incidence at 20 km height has been also assumed. An extended definition of effective cutoff rigidity can be found in (Gerontidou et al., 2021).

A different cosmic ray detector, TRISTAN, of the TRAGALDABAS family, was installed and in operation in the F module of the BAE-JCI from January 2020 to March 2020. It is composed by stacked three planes, each of them divided in a mosaic of 30 rectangular Resistive Plate Chambers (RPCs). Between the second and the third plane there is a 1 cm-thick lead layer covering around a 60% of the surface of the third plane. A detailed description and main results are gathered in Garzón (2020).

2. Observatorio de Rayos Cósmicos Antártico (ORCA)

The Observatorio de Rayos Cósmicos Antártico (ORCA) was installed at BAE-JCI at the beginning of January 2019 after performing a latitudinal survey from Vigo (Spain) to Livingston Island (Antarctica) (Blanco et al., 2019b). ORCA is into a 20 feet container, which is thermally isolated and can be environmentally controlled, named MazORCA. MazORCA has its own power system based on a set of five solar panels and batteries. It also has a communication system consisting of an Iridium Edge transmitter that allows communications via satellite. However, it was decided to connect ORCA directly to the base to ensure a stable power supply and higher bandwidth when sending data. MazORCA functions in this case as an interface between the base and the instruments.

MazORCA is located close to the Scientific module. MazORCA front door points to the scientific module while one of the long sides of the container, the one with solar panels, points to the beach (black container in Fig. 1).

Three detectors constitute ORCA, two neutron monitors and a muon telescope (Blanco et al., 2019a; Ayuso et al., 2021), and a meteorologic station. The detectors share a common structure which keeps the relative position of the different detectors. A picture of the distribution of the ORCA's detectors inside MazORCA is shown in Fig. 2 and a diagram of the distribution of the detectors

Fig. 1. Upper picture: a general view of BAE-JCI. Down picture: MazORCA (the ORCA's black container) close to the scientific module building (red building) and the communication antenna (white igloo).

Fig. 2. MazORCA interior. The control and communications electronics cabinet is in the front, and the structure with ORCA's detectors is in the back.

is shown in Fig. 3. A meteorologic station (Vaisala PTU300 Combined Pressure, Humidity and Temperature Transmitter) provides measurements of pressure, temperature and relative humidity inside MazORCA. The meteorologic station is located in the control and communications cabinet far enough from electronic heat sources. Inside MazORCA, equipment is connected to a local Ethernet network. Data is stored in a common Network-attached storage system (NAS). It can be administered and controlled remotely if required.

2.1. Neutron monitors

ORCA has two neutron monitors. It is foreseen to submit their measurements to the NMDB. Their identifiers in the NMDB will be ORCA and ORCB respectively. Therefore, the observatory and one of the neutron monitors share the same identifier, ORCA.

ORCA follows the NM64 standard (Hatton and Carmichael, 1964; Shea and Smart, 2000), i. e. a counter tube surrounded by a polyethylene moderator, which is in turn enclosed in a lead producer formed by lead rings, and an outer reflector also made of polyethylene. It is composed of three BP-28 counters filled by boron trifluorine. Therefore, it is a 3NM64 set.

ORCB is composed with three bare, i. e. without lead producer or polyethylene, LND2061 counters filled by boron trifluorine. The general characteristics of both counter tubes are listed in Table 1. The two neutron monitors are placed one on top of the other, being ORCA below ORCB (Fig. 3).

The signals from ORCA and ORCB are preprocessed in a signal conditioning system before reaching the data acquisition system. This system consists of a Field Programmable Gate Array (FPGA) with an IP (intellectual property) core specifically designed for this application, and an embedded Linux Beaglebone Black system in which the capture code is executed, as well as the necessary corrections, the editing of the data and its subsequent publication in a database (Población et al., 2014). This system keeps its local clock synchronized using the Network Time Protocol (NTP) server, which is equipped with a Global Positioning System (GPS) receiver. Additionally, it also controls the Vaisala meteorologic station PTU301 Transmitter. The PTU301 probe measures pressures in a range between 500 and 1100 hPa with an accuracy of $\pm 0.05\,hPa$. The temperature/humidity probe composed by a Pt100 RTD Class F0.1 IEC 60751 and Vaisala HUMICAP 180C respectively, measures in a range of $-40°C$ to $+60°C$ with an accuracy of $\pm 0.2°$ and 0 to 100%RH with

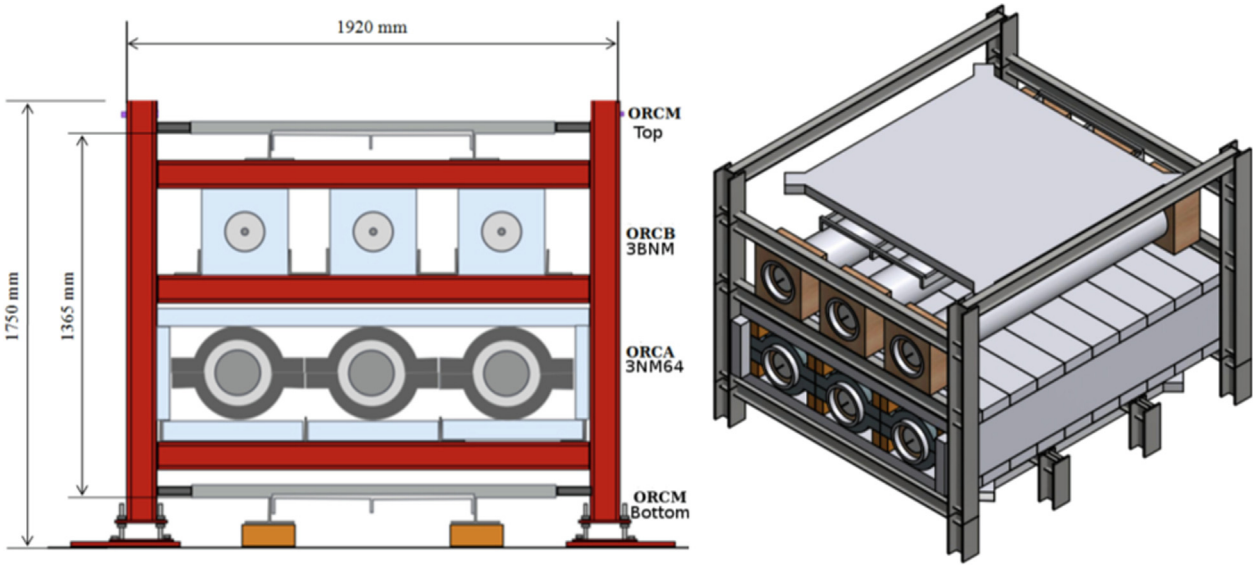

Fig. 3. ORCA diagram. Left: Front view. ORCB grey colored square boxes are 30 cm wide polyspan rings. They fix the bare tubes by the two ends to the structure in their position. Right: Perspective view showing ORCM's top plane and ORCB, ORCA bellow. ORCM's bottom plane is oculted by ORCA body.

Table 1
ORCA/ORCB counter tubes.

Counter Type	BP28	LND2061
Effective diameter (mm)	148.5	149.1
Effective length (mm)	1908.0	1956.3
Cathode material	Stainless steel	Stainless steel
Gas filling	$BF_3(96\%^{10}B)$	$BF_3(96\%^{10}B)$
Gas pressure (mmHg)	200	200
Operational voltage (V)	−2800	1800

an accuracy of $\pm 1\% RH$. Minute averaged measurements from the six counter tubes, the temperature, pressure and humidity sensors are continuously stored in the NAS.

ORCA and ORCB detect neutrons at two different energy thresholds as a consequence of the shielding with polyethylene and lead in ORCA. Once the validity of the measurements of every counter tube is checked, the count rates of both neutron monitors are obtained as the median of the three normalized count rates of each counter, F_1, F_2 and F_3 for the ORCA and A_1, A_2 and A_3 for the ORCB with the formula:

$$F = F_t \times Median\left(\frac{F_1}{\overline{F_1}}, \frac{F_2}{\overline{F_2}}, \frac{F_3}{\overline{F_3}}\right) \quad (1)$$

$$A = A_t \times Median\left(\frac{A_1}{\overline{A_1}}, \frac{A_2}{\overline{A_2}}, \frac{A_3}{\overline{A_3}}\right) \quad (2)$$

where F and A are the count rates for ORCA and ORCB respectively, $F_t = \sum_{i=1}^{3} \overline{F}_i, A_t = \sum_{i=1}^{3} \overline{A}_i$, being $\overline{F}_i$ and $\overline{A}_i$ the average of each counter along the first year of observation.

2.2. Muon telescope

The muon telescope in ORCA is based on the Muon Impact-Tracer Observer (MITO) (Ayuso et al., 2021). This is a telescope composed by a stack of two (Top and Bottom) BC-400 organic scintillators (100 cm × 100 cm × 5 cm, poly-vinyl-toluene with a light output 65% of that of anthracene). Four photomultipliers tubes (PMTs) are coupled to each scintillator by means of a pyramidal light guide. Each PMT collects the light reaching the corresponding lateral surface of the scintillator and generates a pulse whose amplitude is related to the distance between the particle impact point and the corresponding lateral surface of the scintillator (Fig. 4). The particle track is reconstructed by combining the computed impact points at Top and Bottom. Both scintillators are placed at the top and bottom of a metallic structure 136.5 cm apart of each other with ORCB and ORCA in between, and therefore, A 10 cm layer of lead between Top and Bottom (dark grey rings around ORCA tubes in Fig. 3). To follow the nomenclature defined for the neutron monitors (ORCA and ORCB) within the NMDB, MITO is named as ORCM. ORCM provides one minute count rates for four coincidence configurations and particle impact point on each scintillator. The coincidence configurations are: Top: the four PMTs in the upper scintillator, Bottom: the four PMTs in the bottom scintillator, Coin8: the eight PMTs, i.e. particles that cross both scintillators, and Lateral: a combination of two PMTs in the upper scintillator located at a common lateral side and two PMTs in the bottom scintillator but at the opposite lateral side. These four coincidence configurations can be changed to any possible combination of the eight PMTs. Also, the data acquisition system of ORCM is capable of capturing the pulse shape from the eight PMTs for each particle that impacts on the scintillators. In the normal mode of operation, the data acquisition system stores the height of the pulse produced by each one of the PMTs. Additionally, there is a pulse capture mode available that stores the pulse shapes, although this mode cannot be continuously operated due to the large amount of data that it produces. Pulse shape could contain information about the entering particle and multiplicity, but this is something to be investigated in future works. As it was stated above, it is possible to establish a relationship between the particle impact point on the scintillator plane and the light gathered through the opposite lateral sides (Ayuso et al., 2021). A different approach to the estimation of the impact point based on a neural network approach can be found in Regadío et al. (2020).

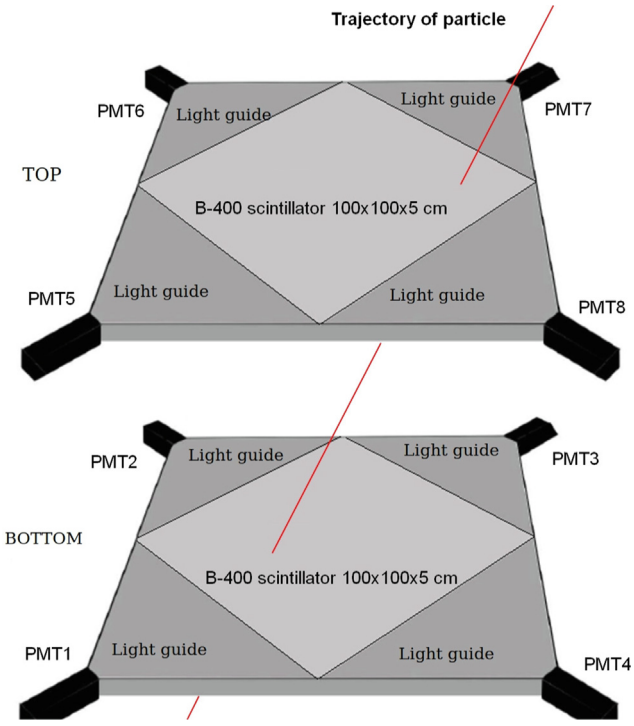

Fig. 4. ORCM scintillator arrangement. Black prisms are the 8 PMTs. The 8 guide lights are in darker grey and scintillators in light grey. This figure has been adapted from Ayuso et al. (2021).

The local coordinate system is defined by the direction of PMT1 to PMT3 and Y axis is defined by the direction of PMT4 to PMT2 (see Fig. 5). Once the x and y coordinates on each scintillator, i. e. Top and Bottom, are obtained, the azimuth ϕ and zenith θ angles that define the particle trajectory can be computed from equations:

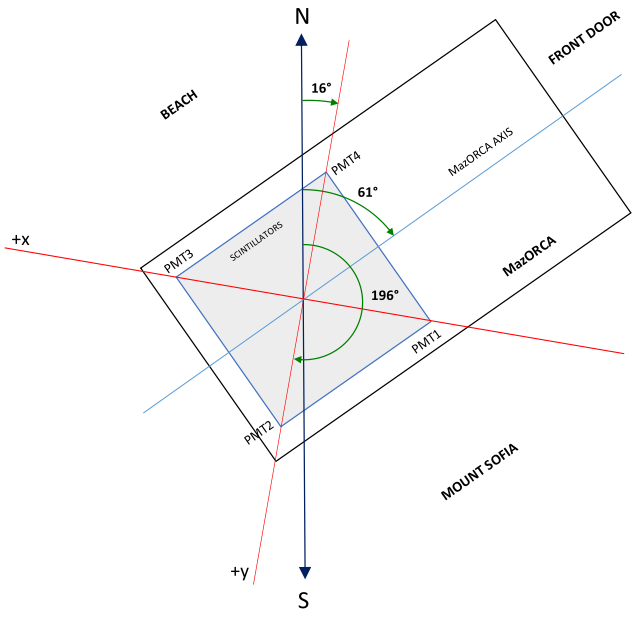

Fig. 5. Zenith view showing MazORCA global orientation with respect geographical North and ORCM relative orientation into MazORCA. The black rectangle represents MazORCA's walls.

$$\phi = \arctan\frac{y_B - y_T}{x_B - x_T} \tag{3}$$

and

$$\theta = \arctan\frac{\sqrt{(x_B - x_T)^2 + (y_B - y_T)^2}}{z} \tag{4}$$

being ϕ the azimuth angle, θ the zenith angle, x_T, x_B, y_T and y_B the x and y coordinates on Top and Bottom respectively. z is the distance between Top and Bottom. The orientation of MazORCA with respect to the geographical North and the local orientation of ORCM local system as is defined above, is shown in Fig. 5. The surroundings, beach, Mount Sofía and front door, are depicted in the figure also.

As an example, a 2D polar histogram for hour nine of the 2020–06-15 data is presented in Fig. 6. Geographical North is at 0 degrees and East is at 90 degrees. The histogram radius represents zenith angle. An expected zenith anisotropy is clearly observed and a slight azimut anisotropy is also observed, although further investigation about the origin of that anisotropy must be completed.

2.3. Detector response

A GEANT4 simulation has been performed to estimate the detector response to the passage of secondary cosmic rays throughout the detector volume (Fig. 7).

To perform the simulation a step by step approach has been followed. Bare $^{10}BF_3$ counters, NM64 standard counters and ORCM were simulated individually first; then, the whole system altogether. Taking into account the features of the scintillators, counter tubes and the characteristics of the walls of the ORCM housing, several Monte Carlo

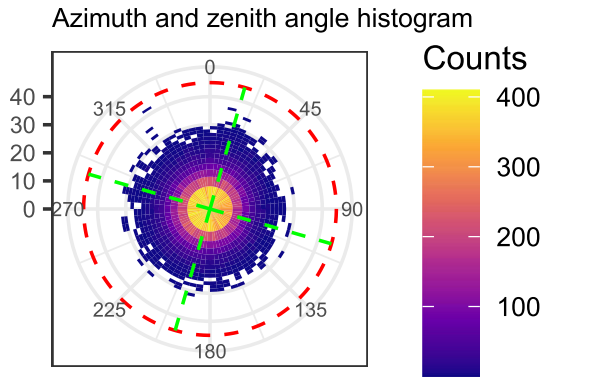

Fig. 6. Polar histogram for an azimuth-zenith grid. Observations are extracted from Coin8, i. e. reconstructed particle trajectories using impact points at Top and Bottom. Data were recorded during the hour 9 of 2020–06-15. Green lines mark the X and Y axis depicted in Fig. 5. North is at 0 degrees.

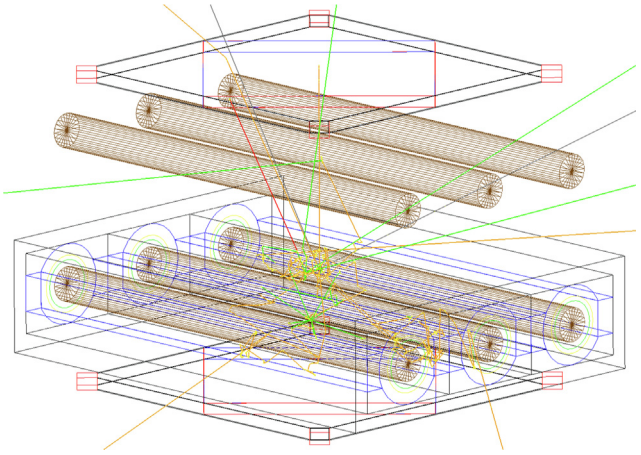

Fig. 7. Example of ORCA Geant 4 simulation. One 100 MeV vertical incident neutron is the primary particle.

simulations were carried out in order to estimate the energy deposited by secondaries into the detector volume and design an algorithm that calculates the coordinates of the muon impact point in the scintillator, based on the pulse levels produced by the PMTs. As an example, a vertical incident 100 MeV neutron has been fired onto the center of the top scintillator (Vertical orange line in Fig. 7). The neutron has a first interaction with the lead of the ORCA module. Multiple secondary neutrons are generated after the neutron-lead interaction and subsequent interaction of these secondary neutrons produce some optical photons, in yellow, gamma rays, in green, and additional neutrons and protons. Some of those secondary particles become in albedo particles for the ORCB module and Top according to this example.

Muons, electrons and protons from 1 MeV to 10 GeV were generated and fired in front of Top at random coordinates and angles of incidence. The kinetic energy losses for muons, protons and electrons when crossing ORCM, the ORCB and the ORCA are on average 350 MeV,

290 MeV and more than 6 GeV respectively. Taking into account the expected energy spectra for these particles at the detector location, the amount of electrons crossing Bottom is negligible.

A vertical incident flat spectrum of neutrons from 1 MeV to 500 MeV was fired to check the response of the ORCA section and also a vertical incident flat spectrum of neutrons from 0.025 eV to 10 MeV to evaluate the response of the ORCB section. Two clear conclusions can be drawn. Although a real expected neutron spectrum has not been used, the highest detection efficiency occurs below 50 eV for the ORCB and above 100 MeV for the ORCA. This is clear in Fig. 8 where the fraction on alpha particle production has been represented for ORCA and ORCB. This preliminary result could establish two different energy thresholds for the detection of neutrons in ORCA.

On the other hand, a significant contribution from neutrons generated in the vicinity of ORCA to the ORCB count rate cannot be ruled out due to the very low energy threshold expected. The complete simulation for the detector response including the expected spectrum of neutrons and the contribution of environmental neutrons will be presented in a future paper.

3. First results

The ORCA observatory has been successfully operating for one year except for eight days in June 2020 and five days in July 2020 when the renewable energy system at the JCI switched off due to the lack of wind and sunlight. It has produced usable data of neutron and muon count rates, incident directions on detector volume and pressure, temperature and humidity from 2020–03-01 to 2021–02-14. ORCA is currently in operation and new data are expected for the next antarctic Spanish campaign at the beginning of 2022.

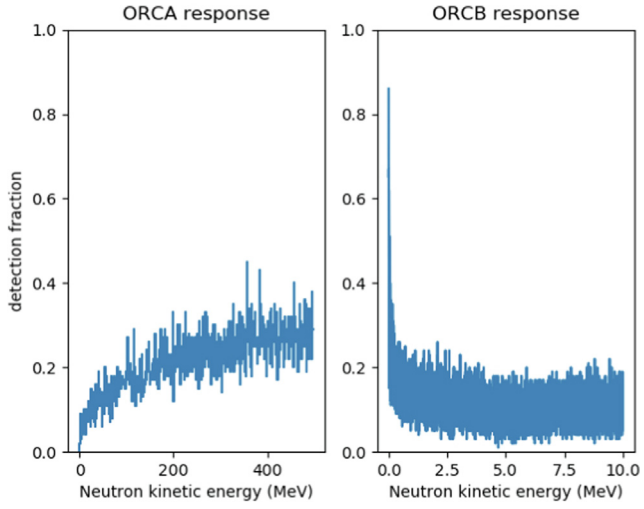

Fig. 8. Fraction of alpha particle production in the $n - {}^{10}B$ reaction inside ORCA (left) and ORCB(right).

3.1. Correlation matrix

The correlation matrix among detector measurements and environmental variables has been computed. It has been computed using hourly data and the most relevant correlations are presented in Table 2. The significance of the correlation coefficients was also estimated using the Monte Carlo approach with artificial series constructed by *the phase randomization procedure* (Ebisuzaki, 1997). The obtained statistical significance (p-value) considers the probability of a random series to have the same or higher absolute value of r as in the case of a tested pair of the original series. The p-values are in the third column of Table 2.

3.2. Correlation among detectors

Our preliminary simulations for the complete observatory, tell us that each detector is more sensitive to different particle populations, ORCA to neutrons above 100 MeV, ORCB to neutrons below 50 eV and ORCM to charged particles, and depending to the used coincidence channel, to different energy thresholds. For instance, Coin8 gathers muons above 200 MeV, protons above 160 MeV and electrons above 5 GeV which means that the main population of particles in Coin8 are secondary muons if the usual cosmic ray spectrum is assumed. Strong correlations among the different count rates could support a common origin of the detected particles, i.e. the primary cosmic ray interaction with atmosphere.

Analysing correlations in Table 2, the high correlation between ORCA and ORCB (r = 0.87) is clear and expected. Top, Bottom and Coin8 have a mean count rate of 11479 min^{-1}, 7774 min^{-1} and 1729 min^{-1} respectively. Coin8 and Bottom show an almost perfect correlation (r = 0.98). This good correlation could be explained if both channels are observing the same population. The difference between count rates, 7774 min^{-1} and 1729 min^{-1}, could reflect the different fields of view of Bottom and Coin8. Additionally, the good correlation could drive to the conclusion that the contribution of albedo particles on Bottom

Table 2
Correlations among measurements. r and p are the correlation factor and the p-value respectively. ORCA and ORCB are the neutron monitors count rates, Coin8 count rate as representative of ORCM, P pressure and T temperature.

Pairs	r	p
ORCA vs ORCB	0.87	< 0.001
ORCA vs Coin8	0.61	< 0.001
ORCA vs P	−0.96	< 0.001
ORCA vs T	0.36	0.008
ORCB vs Coin8	0.43	< 0.001
ORCB vs P	−0.75	< 0.001
ORCB vs T	0.41	0.19
Coin8 vs P	−0.68	< 0.001
Coin8 vs T	−0.21	0.436

measurements are negligible. The bottom scintillator lays on the floor and bellow the lead of ORCA. On the other hand, the correlation between Top and Bottom is very low (r = 0.26), and therefore, so is the correlation between Top and Coin8 (r = 0.20). This correlation and the differences among count rates could be explained because the lower energy threshold in Top and, maybe, an additional non-cosmic contribution. Finally, the correlation between ORCA and Coin8 is moderately high which could indicate that muons and neutrons are produced by the same primary cosmic ray in a large percentage. This leads to the conclusion that the estimation of arrival direction of particles crossing the whole detector could be a reasonable indicator for the primary cosmic ray arrival directions.

3.3. Environmental corrections

Data from neutron monitors and muon telescopes must be corrected according to environmental parameters. Nevertheless, while neutron monitors and muon telescopes are both affected by pressure at the observation site, muon telescopes are also affected by temperature at production height, i. e. the height at which secondary cosmic rays are produced (Lockwood and Calawa, 1957; Mendonça et al., 2013). The dependence between count rates and environmental parameters can be analyzed computing the correlation matrix (Table 2). Although the linear dependence between the logarithm of count rates with respect pressure is known, we prefer to make the comparison among magnitudes to avoid assuming any sort of relationship.

According to Table 2, a high inverse correlation between neutron monitor count rates (ORCA and ORCB) and pressure and a moderate inverse correlation between two ORCM coincidence channels (Bottom and Coin8) and pressure are obtained. The statistically significant in all four cases was higher than 99% ($p < 0.001$). This relationship is well known and is explained by the thickness of the atmosphere through which the secondary cosmic rays pass before arriving at the detector (Lockwood and Calawa, 1957). Most of the correlation coefficients are statistically significant up to at least 99% level, even the small ones $|r| \approx 0.2$. Nevertheless, those related to temperature or relative humidity are either statistically insignificant (although they are low, anyway) or marginally significant, except for 'ORCA vs Temperature" (significant at 99.2% level). It is known that temperature plays a central role at the secondary production height (above 10 km) where it affects the muon production through pion decay. Nevertheless, a direct relation between atmosphere temperature at production height and at sea level is not clear because of the processes responsible of heat exchange between different atmospheric layers (Morozova et al., 2017). This could explain the low correlations and the statistical significance found. We must point out that previous works remark the need of temperature corrections for muon telescopes, therefore, a correlation between temperature and muon count rate must exist (see for instance Mendonça et al. (2013)). This is not clear for ORCM (Table 2). Several reasons can explain the behavior of ORCM. The lack of a link between temperature at secondaries production height and ground level temperature as we have already pointed out above. The even weaker connection between the temperature at production height and the MazORCA indoor temperature which is used in this work or the low variation of temperature into MazORCA along the year, about 10 Celsius degrees in winter, and less in summer when the room temperature control is working. This is an open issue that we must tackle in the near future.

From Table 2 it is inferred that pressure correction is required to remove the effect of the amount of air mass on detector position. This correction eliminates atmospheric effects preserving a count rate that depends only on primary cosmic ray flux at the top of the atmosphere. This correction can be carried out by introducing the β_P factor, which is obtained by fitting the natural logarithm of the count rate with respect to pressure (Lockwood and Calawa, 1957). On the other hand, the low correlation with room temperature suggests that additional temperature corrections are not necessary. This is clear for neutrons. The fit shown in Fig. 10 and the obtained extremely low correlation confirm this.

Finally, it must be pointed out that ORCM count rate could need a temperature at production height correction to remove completely atmospheric effects from muon count rate. These data are not available at this moment so this matter should be addressed in a near future.

The response of the detectors in ORCA with respect to the energy and type of incident particles can result in a change in the ratios between the count rates of the different instruments. These variations can be a consequence of both changes in observing conditions, e.g. snow accumulation, and the effect of solar activity. The ratio between ORCB and ORCA is especially sensitive to these circumstances. It is possible to select periods for which the ratio remains roughly constant. This ensures the elimination of periods affected by environmental conditions or solar activity. This is necessary, in order to determine a correct correction of the measurements as a consequence of the above mentioned pressure effect. Accordingly, a filter based on the ratio between ORCB and ORCA has been applied to select the hours without solar activity or snow presence. This selected period has been used to determine the beta factors,i. e. β_P and β_T. The selection criterion is chosen as $0.125 < ORCB/ORCA \leqslant 0.135$.

The computed β_P and β_T factors for ORCA, ORCB, Top, Bottom and Coin8 are shown in Table 3. Both linear correlation values and fit of $log(N/N_0)\, vs P - P_0$ and $log(N_{Pcorrected}/N_0)\, vs T - T_0$, Tables 2 and 3 respectively, suggest that additional room temperature correction is not needed for any of the detectors integrated in ORCA. The very low correlations and the χ^2/doF confirm that ORCM count rates and room temperature are not related by an exponential law.

Table 3
Pressure and temperatures correction factors. β_P and β_T are the correction factors for pressure and temperature respectively. $R^2 = r^2$ is the determination coefficient being r the correlation factor. χ^2/doF is the chi-squared number for the fits.

Sensor	$\beta_P(hPa^{-1})$	β_P error	R^2	χ^2/doF	$\beta_T(K^{-1})$	β_T error	R^2	χ^2/doF
ORCA	0.00753	±0.00004	0.991	0.00006	−0.000244	±0.00012	0.0098	0.00006
ORCB	0.00720	±0.00006	0.972	0.00016	0.00009	±0.0002	0.0005	0.00016
Top	0.00236	±0.00005	0.849	0.00011	0.0019	±0.00013	0.33	0.00007
Bottom	0.00176	±0.00004	0.796	0.00008	0.0015	±0.00014	0.275	0.00006
Coin8	0.00153	±0.00006	0.611	0.00016	0.0011	±0.00019	0.067	0.00015

As an example, the estimation of the β_P and β_T parameters for the ORCA unit is shown in Fig. 9 and 10. Once the factor β_P is computed the count rate can be corrected using the formula:

$$N_{ic} = N_i \exp(-\beta_{Pi}(P - P_0)) \quad (5)$$

where N_{ic} is the corrected count rate for the observation i, N_i is the uncorrected count rate, P is the pressure and P_0 is the reference pressure. In this work, the reference pressure is the averaged pressure at the detector site along the period of observation. The pressure corrected count rate according Eq. 5 is used to compute β_T in Fig. 10.

3.4. Snow effect

The snow regime precipitation at South Shetland Archipelago is characterized by a smooth increase from the minimum in February to August-September, when the maximum is reached, following a steep decrease to the February minimum. This behavior was reported by de Pablo et al. (2016) on two different observation sites in Livingston and Deception islands. A similar behavior has been confirmed by de Pablo et al. (2020) in a permafrost monitoring site at Deception Island in South Shetland Archipelago for the year 2015. Additionally, the same can be concluded from the Meteoblue simulated climate diagrams based on 30 years of hourly weather model simulations. The diagrams for South Shetland Islands are available at https://www.meteoblue.com/en/weather/historyclimate/climatemodelled/south-shetland-islands_antarctica_6625769. Regarding the snow coverage at BAE-JCI, only from January to March the ground is usually free of snow.

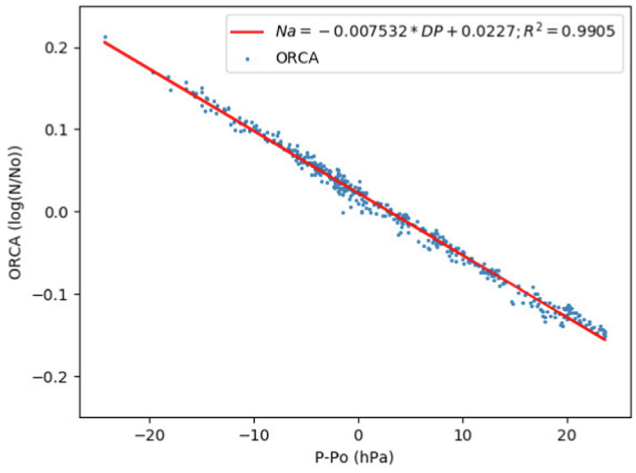

Fig. 9. ORCA count rate-Pressure correction.

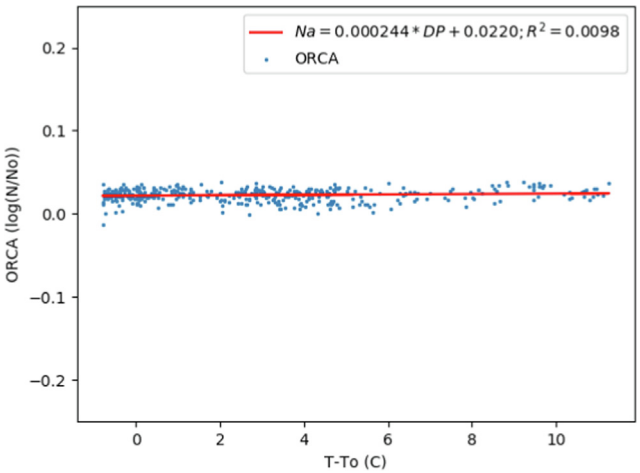

Fig. 10. ORCA count rate-Temperature correction.

The amount of snow over and surrounding ORCA can affect the count rate observed by ORCA, ORCB and the coincidence channels of ORCM Top, Bottom, and Coin8, in different ways. This is clear for neutrons because water interacts effectively with neutrons through the n-p scattering process. Although the interaction with hydrogen in water molecules can result either in an enhancement due to the scatter of incident neutrons toward the detector, or in a decrease caused by absorption, water preferentially attenuates the neutrons (Korotkov et al., 2013). The effect is so important that the presence of snow could nullify comparability over multiyear time series (Usoskin et al., 2017). On the other hand, muons are expected to be less affected or even unaffected by snow covering ORCA because they are more penetrating than neutrons or other secondary cosmic rays.

The first year of daily averaged pressure corrected data from ORCA is presented in Fig. 11. The count rates have been normalized by their own average along the year. ORCA and ORCB (green and red dots respectively) show their higher values on March 2020 and January 2021, in coincidence with periods without snow or with periods with snow precipitation and rapid merging of snow and snowmelt. ORCB is strongly affected by snow coverage showing a continuous decrease from May to November when a minimum is reached. Conversely, the count rate

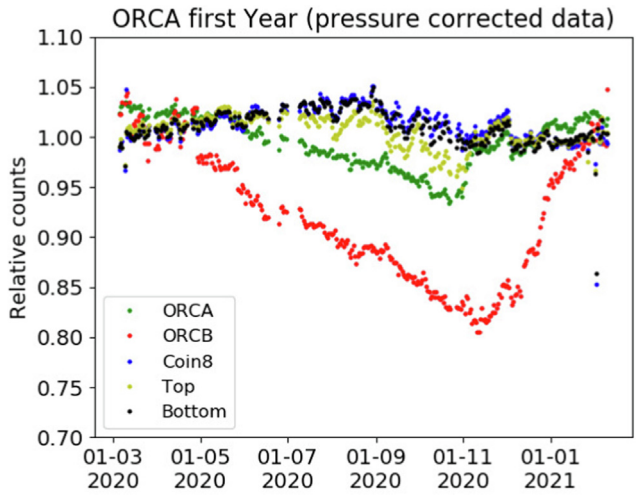

Fig. 11. Pressure corrected normalized count rates of ORCA's instruments.

shows a steeper enhancement from November to March. The effect of snow can be corroborated by comparing the count rates with the snow days curve in de Pablo et al. (2016) where a clear anti-correlation between count rate and snow days is observed. ORCA also shows the snow effect, although more weakly than ORCB. This can be explained by the different energy threshold of neutrons detected in 3NMB and ORCA. The minimum in ORCA is reached early in the year but the global behavior is similar to ORCB. A progressive decrease with a shorter and steeper increase in the count rate afterwards. Regarding ORCM, the snow effect is still observable in Top and almost negligible in Bottom and Coin8. The difference among Top, Bottom and Coin8 could be explained considering the population of the secondary cosmic rays arriving to ORCA. Top detects particles that cannot be observed by bottom because of the huge different energy threshold. Additionally to the snow effect, ORCM coincidence channels show a roughly sinusoidal annual modulation with a maximum around September 2020 and the minimum around January 2021. This observation has to be confirmed when more data will be available.

The different effect of snow on neutron monitors (ORCA and ORCB) and ORCM channels (Top, Bottom and Coin8) count rates could be a way to estimate some properties of snow at the observation site although this is out of the scope of the presented work. Nevertheless, corrections on data, especially for ORCB and ORCA, must be performed to make data comparable in the long term.

3.5. ORCA as cosmic ray observatory

ORCA is a multi-detector instrument designed to measure some of the secondary particles generated during the interaction of cosmic rays with atmospheric atoms. It is clear that atmospheric and snow coverage effects must be removed from the count rates to allow a proper study of the evolution of cosmic rays arriving Earth. The South Pole neutron monitor has two neutron monitors; one of them consists of three ^3He counters and follows the NM64 standard (SOPO), the second one, consisting of 12 ^3He bare detectors (SOPB). The South Pole station is at a cutoff rigidity of 0.1 GV and at a height of 2820 m a.s.l. Although the detectors may not be directly comparable to ORCA's neutron monitors because of their different rigidity and altitude, the opportunity to compare similar detectors makes the attempt worthwhile. SOPO is also interesting for comparison with ORCA because of the small effect that snow has on its measurements. Snow precipitation is very low and the major snow accumulation is due to wind drift from other regions of Antarctica. Because of this, although snow accumulation on the sides of building structures may be greater, snow accumulation on the roof of structures is small or negligible. A discussion of the effect of snow on SOPO measurements can be found at Bieber et al. (2013). Daily averaged data of ORCA and SOPO (bottom panel) and ORCB and SOPB (top panel) are presented in Fig. 12. The effect of snow is clear when comparing ORCB and SOPB as ORCB shows a decrease of about 20%. The same is observed in ORCA vs SOPO but in this case the decrease is about 5%. It has been reported by Korotkov et al. (2013) that short term temporal variations are not affected by the snow layer on neutron monitors. The snow layer results in a general decreased in count rate but relative temporal variations are still preserved. This can be also observed in Fig. 12.

Solar activity along the first year of observations by ORCA has been characterized by being very low. No major solar events happened and, in consequence, neither Forbush decreases, nor ground level enhancements could be observed. This makes it difficult to say that ORCA can observe solar events but the similar behaviour of ORCA when comparing short term variations with SOPO suggest that ORCA will be able to. Recently, a Ground Level

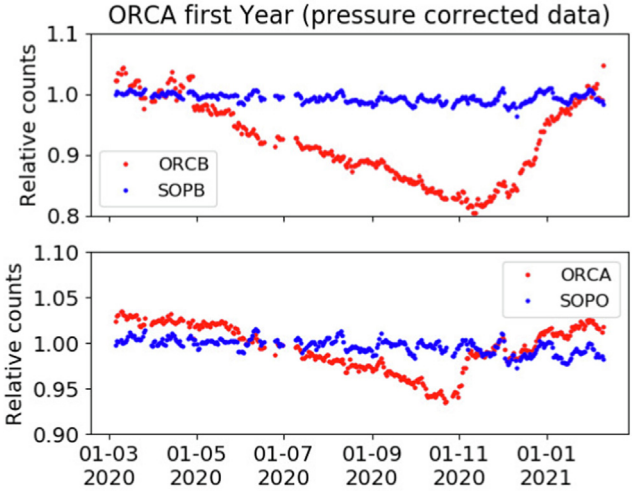

Fig. 12. Pressure corrected normalized count rates of ORCA and SOPO (bottom panel) and ORCB and SOPB top panel.

Enhancement (GLE73) has been observed by low rigidity neutron monitors on 2021/10/28. This GLE73 was followed by a deep Forbush decrease initiated on 2021/11/04. Unfortunately, data from ORCA are not available at the moment of writing this work.

4. Conclusions

ORCA is new detector designed to monitor secondary cosmic rays. It was successfully installed in Juan Carlos I Antarctic Station on January 2019, and since January 2020 it is providing its observations continuously.

ORCA is a combination of neutron monitors and a muon telescope sharing a common housing. This makes it the most complete instrument devoted to the observation of cosmic rays in the range between some GeVs and a few hundreds of GeV.

ORCA provides neutron count rates at two different thresholds, high energy muon count rate, low energy muons, charged particles (electrons mostly), count rates and arrival directions for particles passing through the entire detector.

Snow corrections must be performed to make data comparable with other neutron monitors. This will be performed upon in the near future.

Declaration of Competing Interest

The authors declare that they have no known competing financial interests or personal relationships that could have appeared to influence the work reported in this paper.

Acknowledgments

Thanks to the project PID2019-107806 GB-I00, funded by Ministerio de Ciencia e Innovación. The neutron monitor data from South Pole are provided by the University of Wisconsin, River Falls. Juan José Blanco would like to give special thanks to Dr. Christian T. Steigies for his continued support of our research and his participation in the ORCA installation during the 2018–19 Spanish Antarctic campaign. Finally, the ORCA team wants to thank the BAE Juan Carlos I staff; without their support, the installation and operation of ORCA in Antarctica would have never been possible.

References

Ayuso, S., Blanco, J.J., García-Tejedor, J.I., Gómez-Herrero, R., Vrublevskyy, I., García-Población, O., Medina, J., 2021. Mito: a new directional muon telescope. J. Space Weather Space Clim. 11, 13. https://doi.org/10.1051/swsc/2020079.

Belov, S.M., Zobnin, E., Yanke, V.G., 2021. Cutoff rigidity and particle trajectories online calculator. NMDB@Home 2020: Proceedings of the 1st Virtual Symposium on Cosmic Ray Studies with Neutron Detectors, vol. 1, pp. 197–203. https://doi.org/10.38072/2748-3150/p24. URL: https://macau.uni-kiel.de/receive/macau_mods_00001322.

Bieber, J., Clem, J., Evenson, P., Oh, S., Pyle, R., 2013. Continued decline of South Pole neutron monitor counting rate. J. Geophys. Res.: Space Phys. 118, 6847–6851. https://doi.org/10.1002/2013JA018915.

Blanco, J., García Población, O., García Tejedor, J., Medina, J., Prieto, M., López-Comazzi, A., Ayuso, S., Gómez-Herrero, R., 2019a. A new neutron monitor at the Juan Carlos I Spanish Antarctic Station. In P. Desiati, T. Gaisser, & A. Karle (Eds.), 36th International Cosmic Ray Conference (ICRC2019), volume 1 of Proceedings of Science, pp. 1060.

Blanco, J., García Población, O., García Tejedor, J.I., Steigies, C.T., Medina, J., Prieto, M., López-Comazzi, A., Ayuso, S., Gómez-Herrero, R., Garzón, J.A., García-Castro, D., Cabanelas, P., Gomis-Moreno, A., Villasante-Marcos, V., Heber, B., Morozova, A., Kornakov, G., Kurtukian, T., Blanco, A., Lopes, L., Saravia, J., Kruger, H., Strauss, D.T., Yanke, V.G., 2019b. ORCA (Antarctic Cosmic Ray Observatory): 2018 latitudinal survey. In: Desiati, P., Gaisser, T., Karle, A. (Eds.), 36th International Cosmic Ray Conference (ICRC2019). volume 1 of Proceedings of Science, pp. 1059.

Cordaro, E., Olivares, E., Galvez, D., Salazar-Aravena, D., Laroze, D., 2012. New ^{3}He neutron monitor for chilean cosmic-ray observatories from the altiplanic zone to the antarctic zone. Adv. Space Res. 49, 1670–1683. https://doi.org/10.1016/j.asr.2012.03.015.

De Mendonça, R.R.S., Raulin, J.P., Echer, E., Makhmutov, V.S., Fernandez, G., 2013. Analysis of atmospheric pressure and temperature effects on cosmic ray measurements. J. Geophys. Res.: Space Phys. 118, 1403–1409. https://doi.org/10.1029/2012JA018026, URL: https://agupubs.onlinelibrary.wiley.com/doi/abs/10.1029/2012JA018026. arXiv:https://agupubs.onlinelibrary.wiley.com/doi/pdf/10.1029/2012JA018026.

Ebisuzaki, W., 1997. A method to estimate the statistical significance of a correlation when the data are serially correlated. J. Clim. 10, 2147–2153.

Garzón, J.A., 2020. Trasgos: Towards a new standard for the regular measurement of cosmic. Phys. Atom. Nuclei 83. https://doi.org/10.1134/S1063778820030084, 453–462–174.

Gerontidou, M., Katzourakis, N., Mavromichalaki, H., Yanke, V., Eroshenko, E., 2021. World grid of cosmic ray vertical cut-off rigidity for the last decade. Adv. Space Res. 67, 2231–2240. https://doi.org/10.1016/j.asr.2021.01.011.

Hatton, C.J., Carmichael, H., 1964. Experimental Investigation of the NM-64 Neutron Monitor. Can. J. Phys. 42, 2443–2472. https://doi.org/10.1139/p64-222.

Korotkov, V., Berkova, M., Belov, A., Eroshenko, E., Yanke, V., Pyle, R., 2013. Procedure to emend neutron monitor data that are affected by snow accumulations on and around the detector housing. J. Geophys. Res. Space Phys. 118, 6852–6857. https://doi.org/10.1002/2013JA018647.

Lockwood, J., Calawa, A., 1957. On the barometric pressure coefficient for cosmic-ray neutrons. J. Atmos. Terr. Phys. 11, 23–30. https://doi.org/10.1016/0021-9169(57)90034-X, URL: https://www.sciencedirect.com/science/article/pii/002191695790034X.

Medina, J., Blanco, J.J., García, O., Gómez-Herrero, R., Catalán, E.J., García, I., Hidalgo, M.A., Meziat, D., Prieto, M., Rodríguez-Pacheco, J., Sánchez, S., 2013. Castilla-la mancha neutron monitor. Nucl. Instrum. Methods Phys. Res. A 727, 97–103. https://doi.org/10.1016/j.nima.2013.06.028.

Morozova, A.L., Blanco, J.J., Ribeiro, P., 2017. Modes of temperature and pressure variability in midlatitude troposphere and lower stratosphere in relation to cosmic ray variations. Space Weather 15, 673–690. https://doi.org/10.1002/2016SW001582.

de Pablo, M., Jiménez, J., Ramos, M., Prieto, M., Molina, A., Vieira, G., Hidalgo, M., Fernández, S., Recondo, C., Calleja, J., Peón, J., Corbea-Pérez, A., Maior, C., Morales, M., Mora, C., 2020. Frozen ground and snow cover monitoring in livingston and deception islands, antarctica: preliminary results of the 2015–2019 permasnow project. Geophys. Res. Lett. 46, 187–222. https://doi.org/10.18172/cig.4381.

de Pablo, M.A., Ramos, M., Molina, A., Vieira, G., Hidalgo, M.A., Prieto, M., Jiménez, J.J., Fernández, S., Recondo, C., Calleja, J.F., Peón, J.J., Mora, C., 2016. Frozen ground and snow cover monitoring in the south shetland islands, antarctica: Instrumentation, effects on ground thermal behaviour and future research. Cuadernos de Investigación Geográfica 42, 475–495. https://doi.org/10.18172/cig.2917,

URL: https://publicaciones.unirioja.es/ojs/index.php/cig/article/view/2917.

Población, Ó.G., Blanco, J.J., Gómez-Herrero, R., Steigies, C.T., Medina, J., Tejedor, I.G., Sánchez, S., 2014. Embedded data acquisition system for neutron monitors. J. Instrum. 9. https://doi.org/10.1088/1748-0221/9/08/t08002, T08002–T08002.

Regadío, A., Tejedor], J.I.G., Ayuso, S., Óscar [García Población], Blanco, J.J., Sánchez-Prieto, S., Óscar [Rodriguez Polo], 2020. Trajectory determination of muons using scintillators and a novel self-organizative map. Nucl. Instrum. Methods Phys. Res. A, 973, 164166. https://doi.org/10.1016/j.nima.2020.164166.

Shea, M., Smart, D., 2000. Fifty years of cosmic radiation data. Space Sci. Rev. 93, 229–262. https://doi.org/10.1023/A:1026500713452.

Smart, D.F., Shea, M.A., 1988. Galactic Cosmic Radiation and Solar Energetic Particles. In: Jursa, Adolph S. (Ed.), Handbook of Geophysics and the Space Environment chapter 6, vol. 2. IR Force Geophysics Laboratory, pp. 6.1–6.29.

Thébault, E., Finlay, C.C., Beggan, C.D., Alken, P., Aubert, J., Barrois, O., Bertrand, F., Bondar, T., Boness, A., Brocco, L., Canet, E., Chambodut, A., Chulliat, A., Coïsson, P., Civet, F., Du, A., Fournier, A., Fratter, I., Gillet, N., Hamilton, B., Hamoudi, M., Hulot, G., Jager, T., Korte, M., Kuang, W., Lalanne, X., Langlais, B., Léger, J.-M., Lesur, V., Lowes, F.J., Macmillan, S., Mand ea, M., Manoj, C., Maus, S., Olsen, N., Petrov, V., Ridley, V., Rother, M., Sabaka, T. J., Saturnino, D., Schachtschneider, R., Sirol, O., Tangborn, A., Thomson, A., Tøffner-Clausen, L., Vigneron, P., Wardinski, I., Zvereva, T., 2015. International Geomagnetic Reference Field: the 12th generation. Earth, Planets, and Space, 67, 79. https://doi.org/10.1186/s40623-015-0228-9.

Tsyganenko, N.A., 1989. A magnetospheric magnetic field model with a warped tail current sheet. Planet. Space Sci. 37, 5–20. https://doi.org/10.1016/0032-0633(89)90066-4.

Usoskin, I.G., Gil, A., Kovaltsov, G.A., Mishev, A.L., Mikhailov, V.V., 2017. Heliospheric modulation of cosmic rays during the neutron monitor era: Calibration using pamela data for 2006–2010. J. Geophys. Res.: Space Phys. 122, 3875–3887. https://doi.org/10.1002/2016JA023819, URL: https://agupubs.onlinelibrary.wiley.com/doi/abs/10.1002/2016JA023819. arXiv:https://agupubs.onlinelibrary.wiley.com/doi/pdf/10.1002/2016JA023819..